Catalysis, nanostructure and macroscopic property triangle in bioactive calcium-containing ceramic systems

Anikó Meiszterics [a], Károly Havancsák [b], Katalin Sinkó [a,*]

[a] *Institute of Chemistry, L. Eötvös University, Budapest, H-1117, Hungary*
[b] *Institute of Physics, L. Eötvös University, Budapest, H-1117, Hungary*

ABSTRACT

Calcium silicate ceramics are intended for application as long-term implant materials. In the present work, attention was paid to understand the correlations between the nanostructure (aggregate size, crystallinity, porosity) and the macroscopic properties (solubility in water and simulated body fluids, SBF; hardness) varying the chemical composition. Varying the catalyst (from a base to various acids) during the chemical synthesis was shown to significantly impact on the pore size, crystallinity and mechanical properties. The basic catalyst yields the ceramics with the highest mechanical strength. Ammonia used in 1.0 or 10.0 molar ratio results in bulk ceramics with parameters required for a biomedical application, good hardness (180–200 HV) and low solubility (1–3%) in water and in SBF. The fine porosity (~50 nm) and homogeneous amorphous structure induce good mechanical character.

1. Introduction

The bioactive glass-ceramics and composites have been successfully used for the repair, reconstruction, and replacement of diseased or damaged parts of the body, especially bone or tooth. The most bioactive glasses and ceramics have been based on a silicate network due to the slight and slow solubility of silicates in human body fluid. Hereby these bioactive materials can be used as long-term implants. The bioactivity can be attributed to the bone bonding behavior. On the surface of bioactive materials, a biologically active carbonate hydroxyapatite (HCA) layer forms which provides the bonding interface with the living tissues. The growth rate of the HCA layer mainly depends on the bioactive glass composition and the porosity. The lower SiO_2 and higher CaO contents result in a higher apatite layer growth, while the larger surface area (> natural bone porosity) and smaller pore size reduce the growth rates of the apatite layer [1–7]. Studying the "in vitro behavior" of the glasses indicates that the presence of phosphorus in the glass composition is not an essential requirement for the development of the HCA layer [1–8]. The apatite layer forms in the P_2O_5-free calcium silicate glasses using the phosphorus content present in the in vitro solution.

The gel-derived ceramics have been demonstrated to have better bioactivity than melt-quenched ceramics [9–13]. The better bioactivity can be explained by the great differences in the textural properties (e.g. in the porosity) of the gel- and melt-derived materials [11–13] and the better homogeneity, purity and amorphous feature of the sol–gel ceramics [11–16]. Furthermore, the amount and the position of crystalline particles can be much easier controlled via sol–gel than melting processes.

In our previous work, acid- or base-catalyzed sol–gel routes have been developed for the synthesis of calcium silicate systems [17,18]. The effect of the chemical composition, notably the catalysts on the bond systems has been investigated [19]. The present work focuses on the determination of the correlations between the ceramic nanostructure (particle size, crystallinity, and porosity) and the macroscopic properties (solubility in distilled water and simulated body fluids; hardness) achieved by using various catalysts (ammonia, acetic acid, and phosphoric acid). Dynamic light scattering (DLS) and scanning electron microscopy (SEM) provide the size characterization. The crystalline phases, morphology, and chemical composition of the particles with different shapes have been analyzed by X-ray diffraction (XRD), SEM, Fourier transform infrared spectroscopy (FTIR), and energy dispersive X-ray spectrometer (EDX).

2. Experimental

2.1. Materials and gel synthesis

The calcium silicate gel samples were produced by sol–gel technique starting from tetraethoxysilane (TEOS), $(Si(OC_2H_5)_4$, 98%, Aldrich) and calcium nitrate tetrahydrate, $(Ca(NO_3)_2 \cdot 4H_2O$, 99%, Reanal) as precursors; 1-propanol (at. Aldrich) as solvent; ammonia (25% aqueous solution, Reanal), acetic acid (99–100%, Reanal) and phosphoric acid (85% aqueous solution, Reanal) as catalysts. The syntheses of materials were

* Corresponding author. Tel.: +36 1 3722500; fax: +36 1 3722592.
E-mail address: sinko@chem.elte.hu (K. Sinkó).

carried out by hydrolysis and polycondensation in an organic solution of stoichiometric amounts of the precursors. The rate of the catalyst concentrations (0.50–10.0 mol catalyst/Si) was varied during this synthesis series. The gelation time of starting organic solution was 1 h in basic (NH_3 solution) or in phosphoric acid catalyzed processes, and 24 h in acidic solution (acetic acid). The aging as well as the drying processes were performed at 80 °C [8–10]. The heat treatment i.e. the sintering of ceramic powders was conducted in two steps, first at 600 °C (30 min) and after pressing the pellets (uniaxial pressing at 24.5–39.2 MPa for 15–20 min/pellets) at 700 °C (3 h, 100 °C/min heating and 20 °C/min cooling rates).

2.2. Characterization methods

The aggregate size of ceramics powders has been determined by *dynamical light scattering* (DLS) method. DLS measurements were performed by means of an equipment (Brookhaven) consisting of a BI-200SM goniometer and a BI-9000AT digital correlator. An argon-ion laser (Omnichrome, model 543AP) operating at 488 nm wavelength and emitting vertically polarized light was used as the light source. The signal analyzer was used in real-time "multi tau" mode. In this mode the time axis was logarithmically spaced over an appropriate time interval and the correlator used 218 time channels. The pinhole was 100 μm. The particles were generally dispersed in ethanol for DLS measurements instead of distilled water in order to avoid the aggregation of the particles in distilled water. The number-weighted particle size distribution was detected by DLS.

The particle size and morphology of ceramic powders and sintered pellets have been studied by a FEI Quanta 3D FEG *scanning electron microscope* (SEM). The SEM images were prepared by the Everhart–Thornley secondary electron detector (ETD), its ultimate resolution is 1–2 nm, and the accelerating voltage is 15.0 kV. Since the conductance of the particles investigated is high enough to remove the electric charge accumulated on the surface, the SEM images were performed in high vacuum without any coverage on the specimen surface. For the best SEM visibility, the particles were deposited on a HOPG (graphite) substrate surface. SEM combined with energy disperse X-ray spectroscopy (EDX) is mainly applied for spatially resolved chemical analysis of bulk samples.

Wide-angle x-ray scattering (WAXS) were detected with a 1D MYTHEN detector in HASYLAB of DESY (Hamburg). The WAXS data were collected over the 2θ-range of 7–30° with a step size 0.0212°. Identification of phases was achieved by comparing the diffraction patterns with the standard PDF cards.

The mechanical properties of bulk ceramics were compared with *Vickers hardness* measurements. The compressed tablets were tested with various instruments (an Akashi Microhardness tester, Anton Paar Microhardness tester MHT 4, and Shimadzu DUH-202 tester). A pyramidal diamond indenter was applied to the tablet surface under a load of 0.5–2 N for 15 s. The tests were repeated at three different places 5–20 times for each sample.

The surface area and porosity of ceramic samples were characterized by CCl_4 sorption analysis at 25 °C on an autosorb computer controlled surface analyzer (AUTOSORB-1, Quantachrome or ASAP 2010 Micrometrics). Each sample was degassed for 12 h prior to analysis.

The *solubility* of the ceramics has been investigated in distilled water as well as in simulated body fluid (SBF) [20]. In all cases the sintered bulk samples were soaked for 1–14 days in distilled water and for 3 days in SBF. The drying process took for 2 h at 180 °C and 2 h at 700 °C after distilled water treatment and for 10 days at room temperature after dipping in SBF, respectively. Parallel tests have been carried out on ten samples. Weight changes, chemical surface modification, and the ions eluted into solution (in tissue culture water after 7 days) were fully analyzed.

The ions dissolved in distilled water were analyzed with *total reflection X-ray fluorescence* (TXRF) spectroscopy. The TXRF measurements were performed with an Atomika 8030C (FEI Co.) instrument. The influence of SBF soaking on the surface was monitored by *attenuated total reflectance* (ATR) *Fourier transform infrared* (FTIR) spectroscopy. The FTIR measurements were performed on Bruker IFS 55 instrument with diamond ATR head (PIKE technology). The infrared spectra were collected over the range of 4000–550 cm^{-1} at a resolution of 0.5 cm^{-1}.

3. Result and discussion

The calcium silicate ceramic systems were synthesized by acid- or base-catalyzed sol–gel routes [17,18]. A Ca- and Si-containing colloid (gel or sol) systems form in the first step of the sol–gel method. The ceramic products can be obtained by drying and sintering processes from the gel system. The main reactions of the gelation are the hydrolysis and condensation. The hydrolysis and condensation reactions require acid or base catalysis [17,18].

The previous research has studied the effect of the chemical parameters (e.g. catalysis, Ca/Si and catalyst/Si ratios) and the heat treatment on the bond systems and aggregate structures. The acid-catalyzed reactions produce a gel system with randomly branched network arising from the fast hydrolysis. The base-catalyzed reactions yield a sol system built up from aggregates due to longer hydrolysis time, which can provide the possibility for the aggregation of particles into the most thermodynamically stable arrangement [19]. The NH_3 catalyst favors the formation of $=Si(OSi)_2$ units $(SiO)_2Si(O^-)_2$ or $(SiO)_2Si(OH)_2$. The Ca ions prefer the bond to $=Si(OSi)_2$ units [19]. The Ca ions bond not only to the silicate matrix or silicate anions in a crystalline phase, but also to the carbonate as well as OH ions in the range of 160–500 °C. According to the XRD data, CaO does not form in these sol–gel derived ceramics up to 1000 °C.

3.1. Comparison of various types of catalyst

In Table 1, the porosity data and the particle sizes represent the structural parameters; while the Vickers hardness values (HV) the mechanical properties. For better comparison, the samples of presented investigations were synthesized with the same compositions (1:1:1 molar ratios of Si/Ca/catalyst) and sintered at 700 °C, only the type of catalysts was varied.

The ceramic products prepared by base catalysis possess the best *mechanical strength* (around 200 HV); this result is promising for a biomedical application. The sample of phosphoric acid catalysis shows altering HV values (on average 120 HV) due to the inhomogeneous phase composition (Fig. 1). The acetic acid catalysis produces low HV values (42–52 HV).

The big differences between the HV data may be explained by the *porosity* (Table 1) and the crystalline phases. The porosity of the ceramic systems is one of the important features with respect to the medical application. For comparison, the average specific surface areas of the cancellous and cortical human bone are 50–100 $m^2\ g^{-1}$ [21,22] and 2–40 $m^2\ g^{-1}$ [21,23,24], respectively. The total porosity

Table 1
Structural and mechanical data of ceramic samples synthesized with different catalysts.

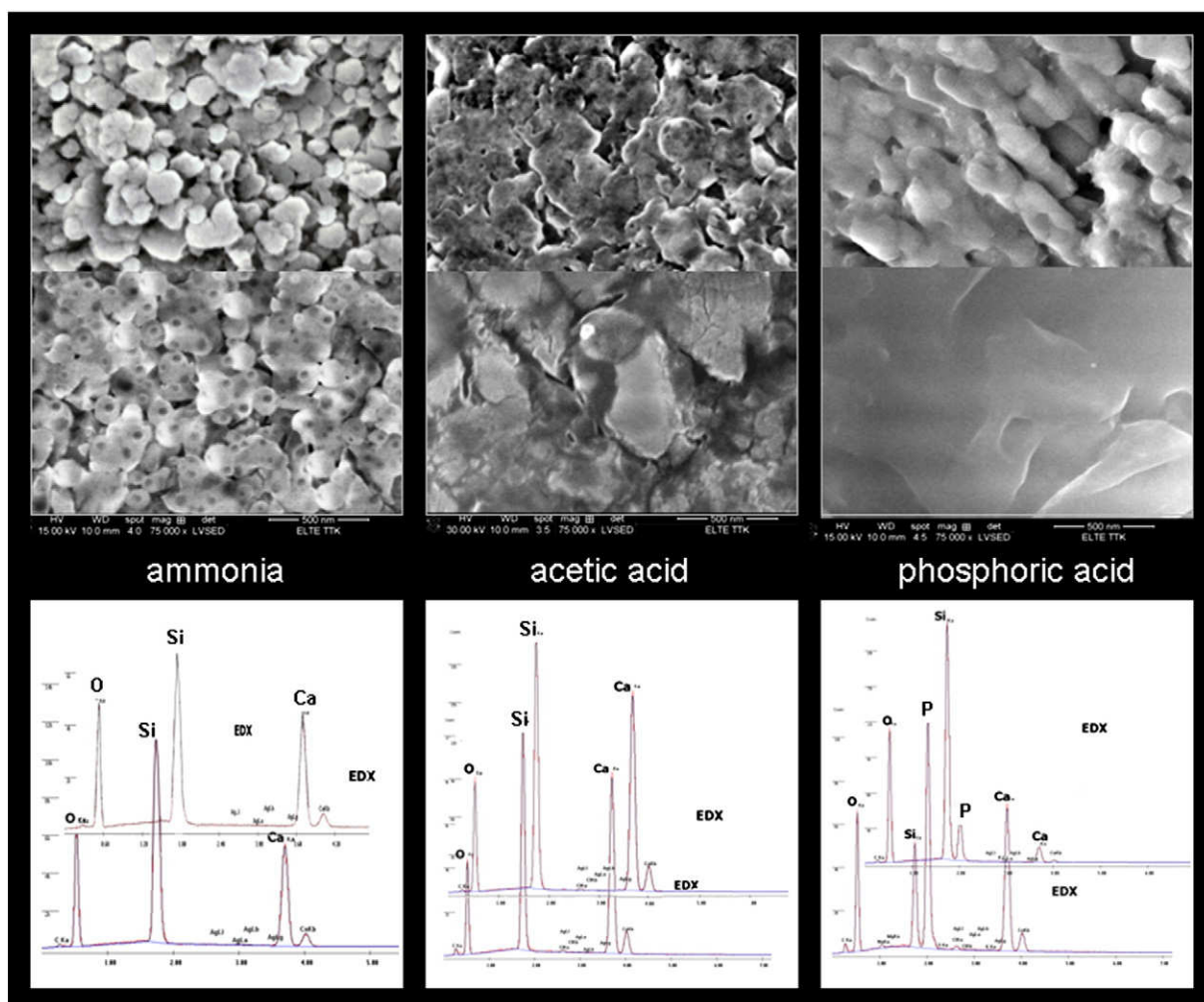| Measurements	Ammonia	Acetic acid	Phosphoric acid
Vickers hardness (HV)	190 ± 20	47 ± 5	120 ± 50
Porosity (%) (SEM)	17 ± 3	8 ± 2	15 ± 2
Specific surface area ($m^2\ g^{-1}$) (CCl_4 adsorption)	19 ± 3	7 ± 2	14 ± 1
Pore size (range/average in nm) (SEM)	20–240/50	20–2000/165	40–1500/310
Particle size (range/average in nm) (DLS)	50–180/90	80–120/100	150–600/300
Particle size (range/average in nm) (SEM)	45–120/75	30–110/90	90–180/119

Fig. 1. SEM images (75 000×) taken from different places of ceramic surfaces formed by means of various catalysts (ammonia, acetic acid, phosphoric acid). EDX spectra illustrate homogeneous (NH_3, HAc) or inhomogeneous (phosphoric acid) chemical composition of the surfaces.

of the cancellous and cortical bone is 30–90% and 5–30% [25–29], respectively. All porosity data fit to the porosity range of natural bone. The highest porosity and the largest specific surface area ($\approx 17\%$, 19 m^2 g^{-1}) could be detected in the samples prepared with ammonia. The ammonia-catalyzed sample contains many fine pores; the mean pore size is about 50 nm. The systems obtained in acidic medium possess the lowest value (8%, 7 m^2 g^{-1}). The acetic acid-catalyzed sample can be characterized by less, but larger and polydisperse pores (20–2000 nm, on average 165 nm). The polydisperse larger pores reduce dramatically the mechanical strength (e.g. ~190 HV at 20–240 nm pore size and ~47 HV at 20–2000 nm). The porosity of the phosphorous containing samples is slightly lower ($\approx 15\%$, 14 m^2 g^{-1}) than that of ammonia catalyzed sample. Whereas, the sample of phosphoric acid has the largest (around 310 nm) but less polydisperse pores, its mean Vickers hardness data is much better than that of acetic acid owing to the glassy phase (Fig. 1). The large pores are present rather in the aggregated part of the bulk ceramics than in glass phases decreasing the mechanical properties of the phase built up from aggregates. Otherwise, the compact and poreless glass phase has a good hardness.

The *size of the particles*, which build up the ceramic structures, has no observable effect on the properties. There is only a slight difference between the particles of base and acetic acid catalysis: 90 (base), 100 (acid) nm before the sintering and 75 (base), 90 (acid) nm after the sintering, respectively) (Table 1). In the sample of the phosphoric acid catalysis, the largest particles (300 nm) can be detected by DLS

before the sintering. After the sintering much lower sizes (119 nm) are presented with SEM. That also indicates that a significant melting process occurred during the sintering at 700 °C.

Comparing the *crystalline structures* obtained by various catalysts, the phosphorous-containing systems possess the largest volume of crystals; β- and γ-$Ca_2P_2O_7$ phases at 700 °C (Fig. 2). On the one hand, the phosphorus content plays an important role in the crystallization of the glasses; it induces the crystallization of calcium phosphate phases. On the other hand, the higher P ratio (>0.5 mol P/Ca) furthers even the melting process. The synthesis with 2 mol P/Ca leads to the formation of a glass foam at 600 °C. Glassy lenses (Fig. 1) are silicate-based glass with 30% phosphorous and 10% calcium oxides content (EDX). In the system of 1:1:1 molar ratio of Ca/Si/P, γ-$Ca_2P_2O_7$ appears first as a crystalline phase during the heating, its amount continually decreases with the rising temperature and turns into β- and γ-$Ca_2P_2O_7$ phases at around 500 °C. A small amount of $CaCO_3$ and 2 $Ca_2SiO_4 \cdot Ca_3(PO_4)_2$ can be identified between 300 and 500 °C. Moreover, the presence of phosphorus produces a heterogeneous distribution of defects in the ceramic bodies reducing the mechanical strength. In the acetic acid-catalyzed systems, a small amount of crystalline phases ($CaCO_3$ and SiO_2) can be demonstrated by XRD or WAXS between 80 and 500 °C. A new calcium silicate phase, β-Ca_2SiO_4 develops already at low temperature (300 °C) that transforms to wollastonite ($CaSiO_3$) at around 900 °C. The ammonia-catalyzed systems are principally amorphous. Only a slight amount of β-Ca_2SiO_4 may be
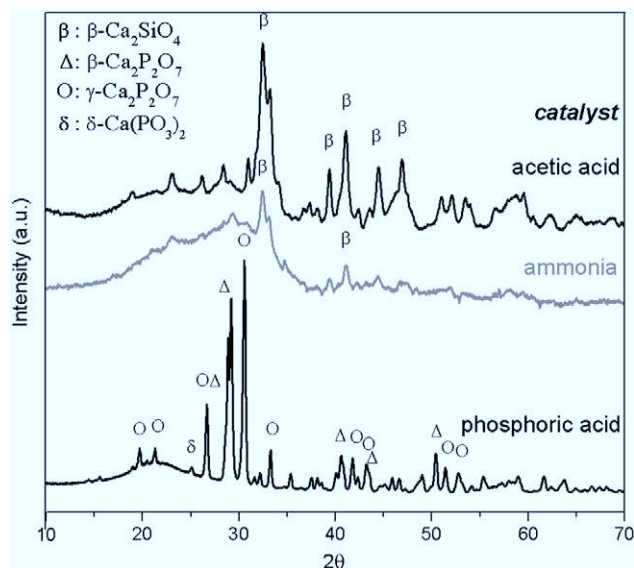
Fig. 2. X-ray diffraction patterns of calcium silicate systems synthesized with different catalysts and heated at 700 °C.

Table 2
Temperature range of the crystalline phases in the function of catalysis.

Temperature range (°C)	Acetic acid	Ammonia	Phosphoric acid
80	$CaCO_3$	Amorphous	γ-$Ca_2P_2O_7$
140	SiO_2		$CaCO_3$
300			$2Ca_2SiO_4 \cdot Ca_3(PO_4)_2$
500	$CaCO_3$	$CaCO_3$	γ-$Ca_2P_2O_7$
	SiO_2	SiO_2	β-$Ca_2P_2O_7$
	β-Ca_2SiO_4		$CaCO_3$
			$2Ca_2SiO_4 \cdot Ca_3(PO_4)_2$
600	β-Ca_2SiO_4	Amorphous	β-$Ca_2P_2O_7$
700		β-Ca_2SiO_4	γ-$Ca_2P_2O_7$
800			δ-$Ca(PO_3)_2$
900	$CaSiO_3$	$CaSiO_3$	
>900			β-$Ca_2P_2O_7$
			SiO_2

observed between 700 and 900 °C (Table 2). Similar to the acetic acid-catalyzed systems, β-Ca_2SiO_4 changes to a calcium metasilicate phase at about 900 °C.

3.2. Material features in the function of ammonia concentration

Only the ammonia-catalyzed bulk ceramics can be utilized as a ceramic body of long-term implants owing to their good bioactivity, sufficient mechanical strength, and low solubility (see in Section 3.3). The phosphorus content provided by H_3PO_4 increases drastically the solubility (discussed further in Section 3.3), while the acetic acid catalysis yields ceramics with low mechanical strength. The previous examinations of the ammonia influence on the bond system have indicated a considerable change at ≥ 1 molar ratio of NH_3/Ca. This ratio of catalyst is needed for achieving the pH required for the hydrolysis

and condensation of TEOS and for the development of Si–OH groups [19]. Thus, the present study focused on the investigations of 1.0–10.0 molar ratios of NH_3/Ca. The structural (porosity, pore and particle sizes) and mechanical parameters (hardness) are listed in Table 3 in the function of ammonia molar ratio. Significant differences can be observed in the Vickers hardness data. The application of terminal (1.0 or 10.0) ammonia molar ratios leaded to surprise results; that produced bulk ceramics with the largest hardness (140–350 HV, on average 180–190 HV). The intermediate ammonia molar ratios provided the bulk ceramics with less hardness (on average 110–120 HV). These data have been checked by three different Vickers hardness testers in order to approve the non-linear change (Fig. 3). The change of HV values can be interpreted by means of porosity, especially of pore size and crystallinity similar to the effect of the various types of catalyst (Table 3). The fine pores (on average 50 nm) result in a good mechanical strength. At 3.0 or 5.0 ammonia molar ratio, the larger pores (on average 80–120 nm) decrease strongly the hardness. The percent porosity and the particle sizes do not change unambiguously as a function of ammonia ratio (Table 3).

The difference in the hardness values can be interpreted by the crystalline phases. The in-situ WAXS and XRD measurements detected α-quartz (SiO_2) and calcite ($CaCO_3$) as first crystalline phases in the ammonia-catalyzed systems during the heat treatment, in the range of 140 and 500 °C (Table 4). Both phases disappear simultaneously at around 500 °C, indicating a reaction between them independent of the ammonia concentration. The character of the newly developed phase depends on the ammonia concentration. The use of 1.0 and 10.0 molar ratios leads directly to the formation of a temporary calcium silicate amorphous phase, which transforms to smaller crystals (β-Ca_2SiO_4) only at higher temperature (700 and 800 °C). The same crystalline phase (β-Ca_2SiO_4) forms already above 500 °C in the samples of the intermediate molar ratios (3, 5). Above 800 °C, β-dicalcium silicate turns into a crystalline phase of calcium metasilicates (e.g. wollastonite) in every sample. Fig. 4 depicts the X-ray diffraction patterns for ceramic systems obtained by using various ammonia concentrations and heated at 700 °C. The XRD curves represent a rising amorphous character for ammonia-catalyzed ceramic materials in the function of the increasing molar ratio.

3.3. Soluble behavior of the sintered calcium-containing ceramic systems

From the view point of medical application, the soluble behavior of the bulk ceramic samples possesses an outstanding relevance. The bulk ceramics sintered at 700 °C were soaked in distilled water as well as in simulated body fluids (SBF). The solubility in distilled water has been characterized by measurements of weight loss and analyzed for ionic content by TXRF after 7 days. The behavior of the bulk ceramics in SBF has been mostly analyzed by surface control (SEM, EDX, FTIR).

A weight loss of 3–4% in distilled water can be detected in the samples synthesized with acetic acid or ammonia catalyst (Table 5 and Fig. 5). These weight losses occur in 1–2 days and after that the bulks hold their weight. In order to determine the reason of weight loss, the chemical composition of distilled water has been analyzed by TXRF measurements observed after a period of soaking in water

Table 3
Structural and mechanical data of ceramic samples synthesized with various amounts of ammonia catalyst.

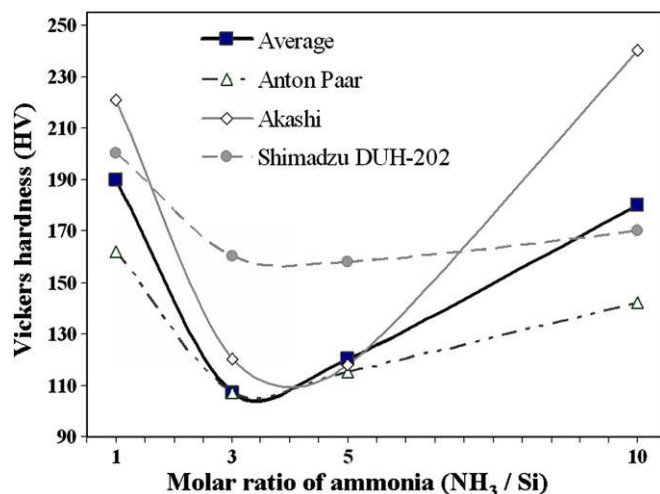| Measurements	Molar ratio of NH_3/Ca			
	1.0	3.0	5.0	10.0
Vickers hardness (HV)	150–240/190	90–120/107	100–180/120	140–350/180
Porosity (%) (SEM)	17 ± 3	15 ± 2	19 ± 3	20 ± 3
Pore size (range/average in nm) (SEM)	20–240/50	20–300/83	10–300/120	5–140/50
Particle size (range/average in nm) (DLS)	50–180/90	30–180/85	35–180/85	30–300/110
Particle size (range/average in nm) (SEM)	45–120/75	50–140/80	45–134/80	45–120/84

Fig. 3. Vickers hardness data measured by different instruments (Anton Paar Micro; Akashi Micro; Shimadzu DUH-202 hardness testers) in the function of ammonia concentration.
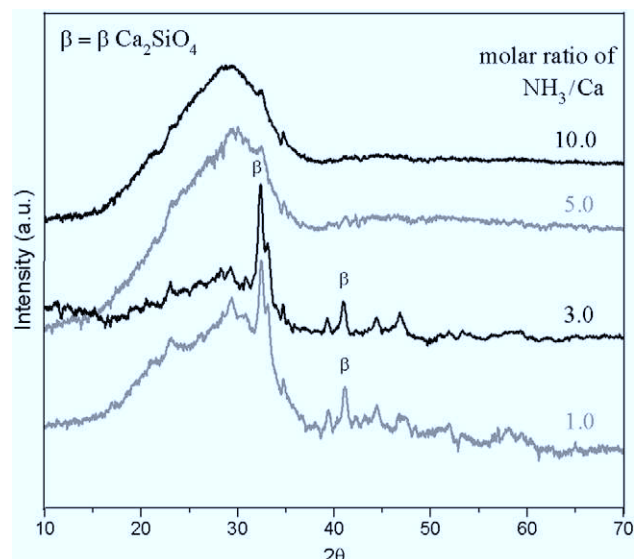

Fig. 4. X-ray diffraction patterns of calcium silicate systems synthesized by various amounts of ammonia catalyst.

after 7 days (Table 6). In acetic acid-catalyzed ceramics, the weight loss ($\approx 4\%$) mostly arises from the dissolution of calcium ions (0.02 g Ca ions/g sample). The solution of the silicon atoms is negligible ($1.7 \cdot 10^{-5}$ g/g sample). After soaking the samples synthesized in basic medium, not only calcium ions ($2.9 \cdot 10^{-3}$–$3.5 \cdot 10^{-3}$ g/g sample) but silicon atoms could also be detected ($1.7 \cdot 10^{-3}$ g/g sample) in the distilled water solution. Considering these concentration data, the major part of the weight loss arises from the sintering defects, i.e. the fine particles can be released from ceramic surfaces. Only a minor part of the weight loss is the consequence of a real water solubility.

In contrast to these acetic acid- or ammonia-catalyzed ceramic materials, a larger and more or less continuous weight loss can be observed in the systems catalyzed by phosphoric acid (Table 5, Fig. 5). The weight change is faster in the first three days and it still continues slower in the second week (Fig. 5). The solubility of the ceramics increases drastically (from 10 to 48%) by rising molar ratio of Si/P (Table 5). The phosphorus-containing systems release mainly phosphorus ($3.7 \cdot 10^{-3}$ g/g sample) and calcium ($2.4 \cdot 10^{-3}$ g/g sample) ions and only a slight volume of silicon ($3.6 \cdot 10^{-4}$ g/g sample) during the soaking (Table 6). The most removed calcium ions (generally 70–80%) are substituted by H^+ ions. The silicon content dissolves as silicon-dioxide from the surface of the phosphoric acid-catalyzed samples.

The weight change of the bulk ceramics has also been investigated after a 3-day soaking in SBF. After soaking and drying, a lower weight growth can be observed; at NH_3 (2–2.5%) and at acetic acid catalysis (5.0–5.5%). The phosphoric acid-catalyzed samples produce low weight losses (2.0–2.5%) by soaking in SBF due to the larger dissolution than the precipitation from SBF. The influence of the soaking in

SBF on the surfaces was compared by means of SEM images (Figs. 6–8) and the adsorbed compounds were identified by EDX analysis. The ~5% weight growth of acetic acid-catalyzed sample occurred by soaking is derived mainly from calcium carbonate and in a smaller part from calcium phosphate and hydroxyapatite precipitation. The small white particles (~350 nm) on the surfaces of acetic acid-catalyzed samples are calcium phosphate crystallites (Fig. 6). The phosphate precipitates are dispersed on the whole surface. The larger crystallites, the "rose" (60–120 μm) proved to be calcium carbonate (Fig. 6).

In the ceramic systems catalyzed by ammonia, a weight growth of 2% can be observed. The precipitates dispersed overall on the ceramic surfaces are similar to that separated in the systems of acetic acid catalyst (Fig. 7). The small phosphate particles (~350 nm) are dominant, while the large carbonate participates (65–120 μm) are present only

Table 4
Temperature range of the crystalline phases in the function of ammonia concentration.

Temperature range (°C)	Molar ratio of NH_3/Ca			
	1.0	3.0	5.0	10.0
80	Amorphous	Amorphous	Amorphous	$Ca(NO_3)_2$
140	$CaCO_3$		$CaCO_3$	$CaCO_3$
	SiO_2		SiO_2	SiO_2
500		$CaCO_3$	Amorphous	
		SiO_2		
600	Amorphous	β-Ca_2SiO_4	β-Ca_2SiO_4	Amorphous
700	β-Ca_2SiO_4			
800				
900	$CaSiO_3$	$CaSiO_3$	$CaSiO_3$	$CaSiO_3$
>900				

Table 5
The time dependence of solubility in distilled water.

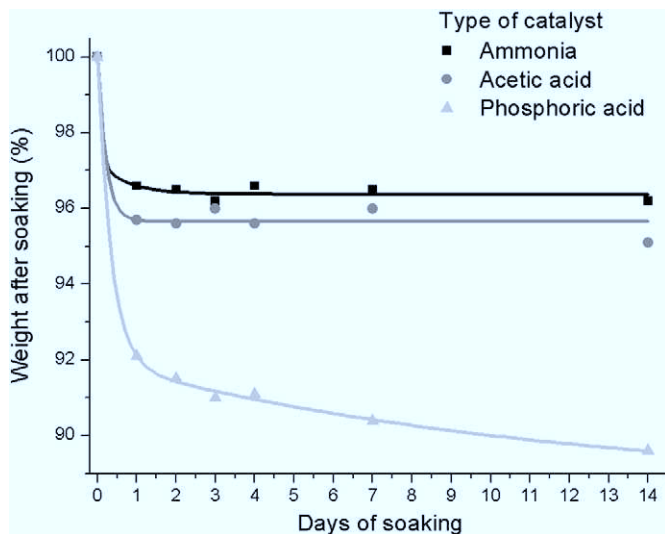| Molar ratio of catalyst/Ca	Days of soaking	Weight loss %	Molar ratio of catalyst/Ca	Days of soaking	Weight loss %
NH_3/Ca = 1	1	3.4 ± 0.4	NH_3/Ca = 1	1	3.4 ± 0.4
	2	3.5 ± 0.5		2	3.5 ± 0.5
	3	3.8 ± 0.4		3	3.8 ± 0.4
	4	3.4 ± 0.3		4	3.4 ± 0.3
	7	3.5 ± 0.3		7	3.5 ± 0.3
	14	3.8 ± 0.3		14	3.8 ± 0.3
CH_3COOH/Ca = 1	1	4.3 ± 0.5	NH_3/Ca = 3	1	4.0 ± 0.5
	2	4.4 ± 0.5		2	3.3 ± 0.5
	3	4.0 ± 0.4		3	4.0 ± 0.4
	4	4.4 ± 0.3		4	3.7 ± 0.4
	7	4.0 ± 0.3		7	4.3 ± 0.3
	14	4.9 ± 0.5		14	4.4 ± 0.3
H_3PO_4/Ca = 1	1	7.9 ± 0.6	NH_3/Ca = 5	1	4.0 ± 0.5
	2	8.5 ± 0.7		2	3.7 ± 0.5
	3	9.0 ± 0.7		3	4.3 ± 0.4
	4	8.9 ± 0.6		4	5.0 ± 0.5
	7	9.6 ± 0.6		7	4.4 ± 0.4
	14	10.4 ± 0.7		14	4.5 ± 0.5
H_3PO_4/Ca = 2	1	40 ± 4	NH_3/Ca = 10	1	4.2 ± 0.4
	2	43 ± 4		2	4.3 ± 0.4
	3	45 ± 4		3	4.3 ± 0.4
	4	45 ± 4		4	4.0 ± 0.4
	7	47 ± 5		7	3.8 ± 0.3
	14	48 ± 5		14	3.9 ± 0.4

Fig. 5. Time dependence of solubility in distilled water.

Table 6
TXRF analysis of the chemical composition of water after a 7-day soaking.

Molar ratio of catalyst/Ca	Ca (g/g)	Si (g/g)	P (g/g)
1.0 acetic acid	$2.0 \cdot 10^{-2}$	$1.7 \cdot 10^{-5}$	–
1.0 H_3PO_4	$2.4 \cdot 10^{-3}$	$3.6 \cdot 10^{-4}$	$3.7 \cdot 10^{-3}$
1.0 NH_3	$2.9 \cdot 10^{-3}$	$1.7 \cdot 10^{-3}$	–
5.0 NH_3	$3.4 \cdot 10^{-3}$	$2.5 \cdot 10^{-3}$	–
10.0 NH_3	$3.5 \cdot 10^{-3}$	$2.3 \cdot 10^{-3}$	–

in a small amount (Fig. 7). Hydroxyapatite precipitation is not carried out.

Relevant changes cannot be observed on the surface of the phosphoric acid-catalyzed samples (Fig. 8). Some phosphate precipitates can be monitored by SEM on certain parts of the surface (Fig. 8). The solubility of phosphate-containing materials is significantly less in SBF (2–3%) than in pure water (8–10%). The reason of that is the Ca^{2+} and PO_4^{3-} ions of SBF decreasing strongly the solubility. However, the precipitation from SBF must also be taken into account.

The FTIR spectra recorded before and after soaking in SBF verified the results of EDX measurements (Fig. 9). In the case of acetic acid and ammonia catalysis, new peaks appear in the FTIR spectra after a soaking in SBF, which can be associated to the phosphate group (PO_4^{3-}, 1080 and 1220 cm^{-1}). Parallel with the absorption of phosphate groups, slight carbonation (1440 cm^{-1} and 670 cm^{-1}) and hydration (1645 cm^{-1}) processes can be identified. In the sample prepared by phosphoric acid, only slight changes can be detected by FTIR after the SBF-soaking. In the FTIR spectrum for the sample derived from the surface layer of an ammonia-catalyzed system, the absorption band of Ca–O–Si strongly reduces and the common band of SiO_4 and PO_4 (1077 cm^{-1}) increases. The decrease of the peak of Ca–O–Si (881 cm^{-1}) indicates the dissolution of the Ca^{2+} ions from the ceramic surface. The calcium ions dissolved in SBF solution are substituted by H^+ ion and produce silanol (Si–OH) groups on the ceramic surfaces. The substitution has been confirmed by the appearance of the OH band in the IR spectra (at 3734 and 1644 cm^{-1}). The silanol group on the surface of biomaterials is reported to be essential for the formation of hydroxyapatite. The silanol group provides favorable sites for hydroxyapatite nucleation [9–13,20,30–34]. The hydroxyapatite-like layer ensures the good connection to the living tissues and increases hereby the bioactivity of ceramics.
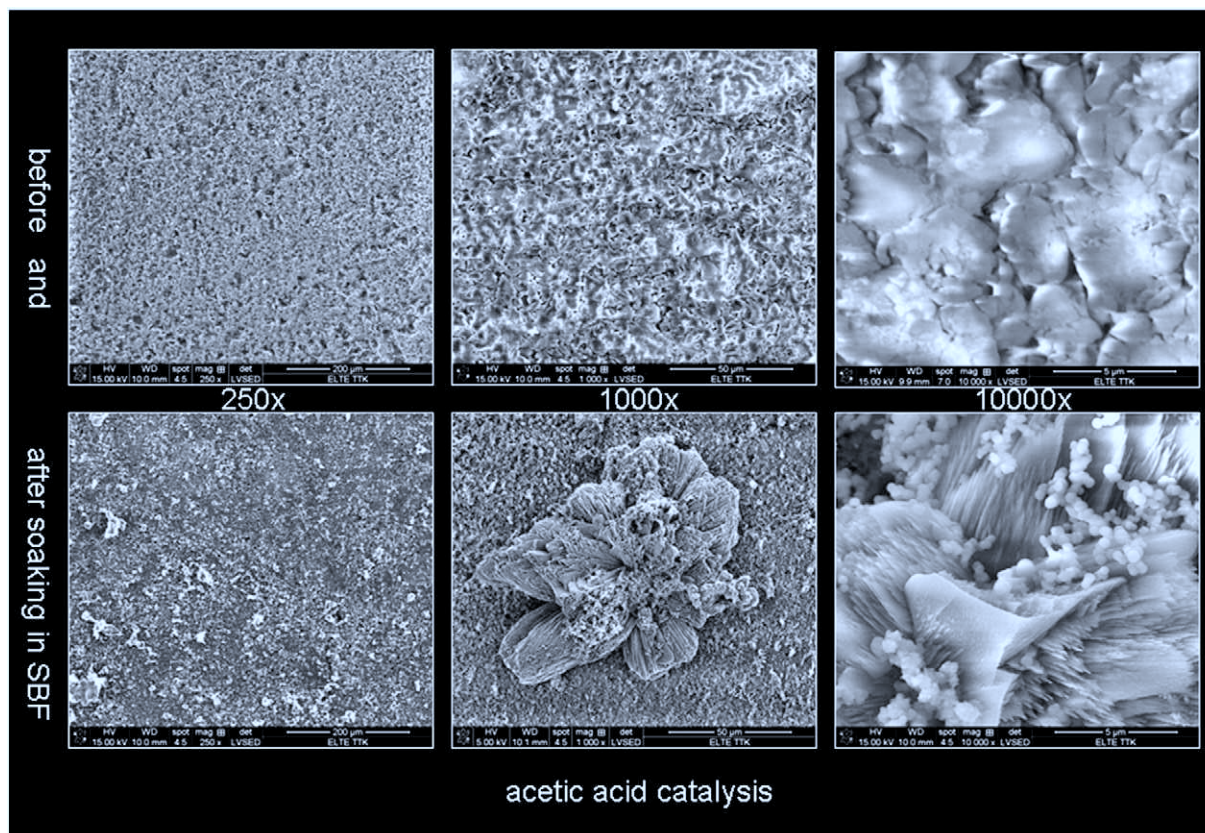

Fig. 6. SEM images of various magnifications for acetic acid-catalyzed samples before and after soaking in SBF for 3 days.
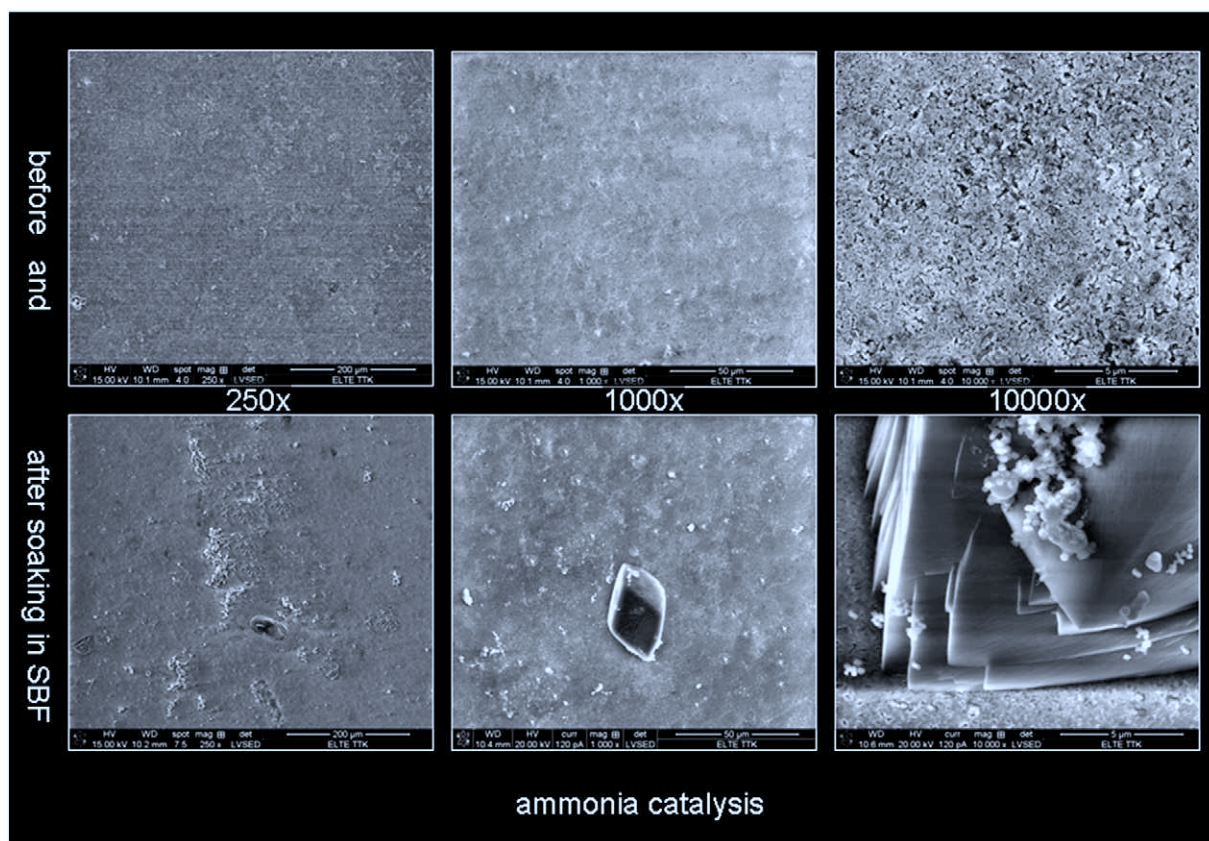
Fig. 7. SEM images of various magnifications for ammonia-catalyzed samples before and after soaking in SBF for 3 days.
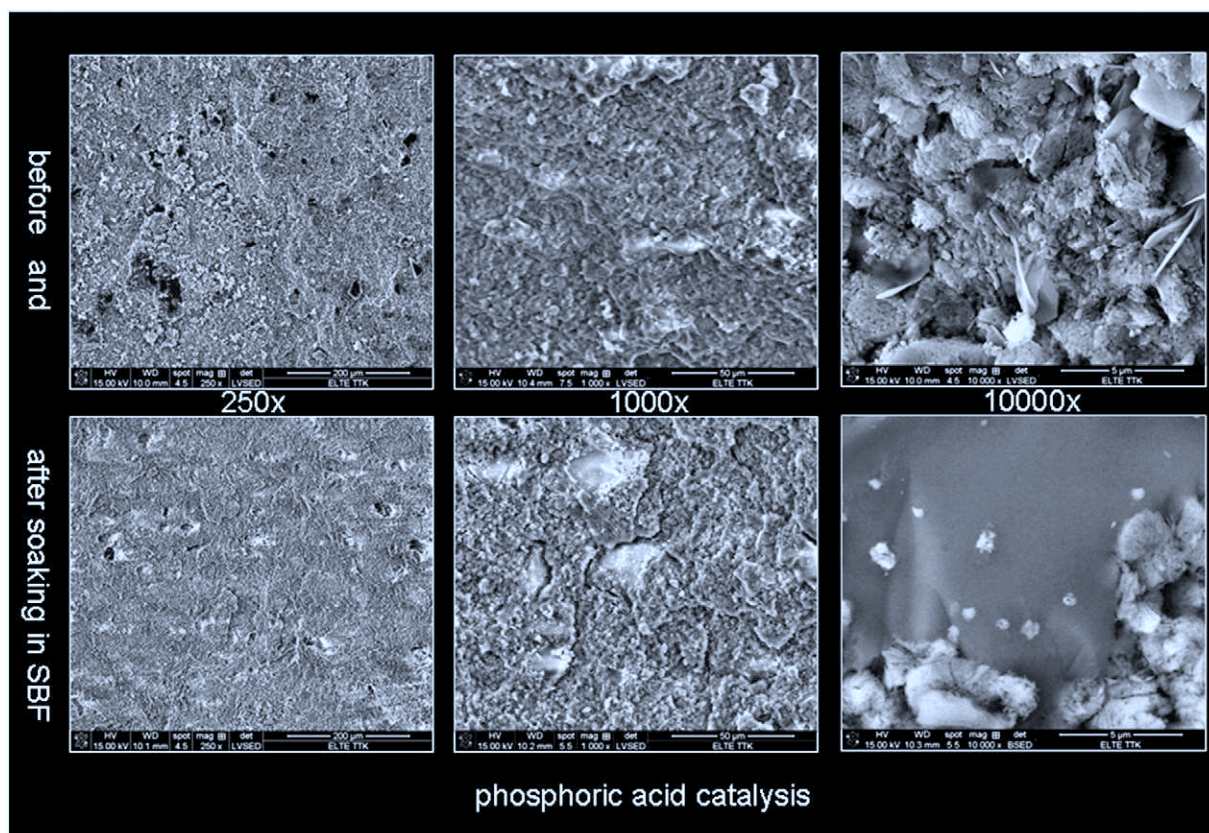

Fig. 8. SEM images of various magnifications for phosphoric acid-catalyzed samples before and after soaking in SBF for 3 days.

The big differences in the mechanical properties may be explained by the porosity, especially by the pore sizes. The large (>100 nm) and polydisperse pores considerably reduce the mechanical strength. However, the large pores (50–100 μm) are crucial for an excellent osteointegration. The pore system desired for the fast osteointegration could be prepared only on the surface of the ceramic body considering the requirement of the long-term implants for the good mechanical strength. The crystallinity has also effect on the hardness, the larger crystals (>100 nm) distort the homogeneous texture and decrease the mechanical strength.

The treatment of calcium silicate bioceramics in SBF leads to precipitation of phosphate and slight carbonate particles. The calcium ions released in SBF solution are replaced by H^+ ion and produce silanol (Si-OH) groups. The silanol groups on the ceramic surface are essential for the formation of hydroxyapatite, hereby improving the bioactivity.

4. Conclusions

The bioceramics based on silicate matrix can be utilized as long-term implants due to their slight and slow solubility of silicates in the human body fluid. The aims of the present work were to synthesize bulk calcium silicate bioceramics by new sol–gel route and to understand the correlations between the nanostructure (porosity, morphology or aggregate size) and the macroscopic properties (solubility in water and simulated body fluids, SBF; Vickers-hardness, HV). Varying the preparation conditions, the catalyst proved to be the most efficient parameter in the influence of the ceramic structure and mechanical properties. Basic (NH_3) and acidic (CH_3COOH, H_3PO_4) catalysts were applied in the research work.

Ammonia of the different catalysts provides the bulk ceramics with good mechanical properties and low solubility required for a biomedical application. The ammonia-catalyzed systems are principally amorphous. The fine porosity (~50 nm) induces the good mechanical character. The ceramic properties depend not only on the type of catalyst but ammonia concentration, too. The ammonia catalyst used in 1.0 or

10.0 mole ratio of NH_3/Ca results in the largest hardness (~200 HV), similar porosity (17-20%) to that of human cortical bone and low solubility (1-3%) in water and SBF. The use of 1.0 or 10.0 molar ratio leads directly to the formation of a temporary calcium silicate amorphous phase, which transforms to smaller crystals (β-Ca_2SiO_4) only at higher temperature (around 700 °C).

In the respect of biomedical application, the main disadvantage of the acetic acid-catalyzed systems is their bed mechanical strength (45–50 HV). The reduction of the mechanical strength derives from the larger and polydisperse pores (20–2000 nm, on average 165 nm). The characteristic crystalline phase is β-Ca_2SiO_4 formed at 300 °C and the crystals are growing up to the temperature of sintering. The advantages of the bulk ceramics catalyzed by acetic acid are the homogeneous gel structure, low solubility (~4%) in water and SBF, and an apatite layer can be formed on their surface in SBF.

The phosphoric acid-catalyzed ceramic systems can not be utilized as an implant owing to their inhomogeneous structure and larger and long term solution in water. The solubility of the ceramics increases drastically by rising molar ratio of P/Si. The phosphorous-containing systems possess the largest volume of crystals; β- and γ-$Ca_2P_2O_7$ phases. Over the crystalline phases, glassy lenses can be displayed in the texture. The inhomogeneous structure results in changing HV values (on average 120 HV). The pores in the samples of phosphoric acid are generally large (~310 nm) but less polydisperse.

References

[1] I. Izquierdo-Barba, A.J. Salinas, M. Vallet-Regi, J. Biomed. Mater. Res. 47 (1999) 243–250.
[2] A. Martínez, I. Izquierdo-Barba, M. Vallet-Regi, Chem. Mater. 12 (2000) 3080–3088.
[3] A.J. Salinas, M. Vallet-Regí, I. Izquierdo-Barba, J. Sol-Gel Sci. Technol. 21 (2001) 13–25.
[4] M. Vallet-Regi, V.C. Ragel, A.J. Salinas, Eur. J. Inorg. Chem. 2003 (2003) 1029–1042.
[5] N. Olmo, A.I. Martín, A.J. Salinas, J. Turnay, M. Vallet-Regí, M.A. Lizarbe, Biomaterials 24 (2003) 3383–3393.
[6] M. Vallet-Regi, A.J. Salinas, A. Martínez, I. Izquierdo-Barba, J. Pérez-Pariente, Solid State Ionics 172 (2004) 441–444.
[7] H. Yan, K. Zhang, C.F. Blanford, L.F. Francis, A. Stein, Chem. Mater. 13 (2001) 1374–1382.
[8] T. Kokubo, J. Non-Cryst. Solids 120 (1990) 138–151.
[9] M. Catauro, G. Laudisio, J. Sol-Gel Sci. Technol. 10 (1997) 231–237.
[10] M.I. Alemany, P. Velasquez, M.A. de la Casa-Lillo, P.N. De Aza, J. Non-Cryst. Solids 351 (2005) 1716–1726.
[11] M. Vallet-Regí, A. Rámila, Chem. Mater. 12 (2000) 961–965.
[12] J. Pérez-Pariente, F. Balas, M. Vallet-Regí, Chem. Mater. 12 (2000) 750–755.
[13] M. Vallet-Regí, D. Arcos, J. Pérez-Pariente, J. Biomed. Mater. Res. 51 (2000) 23–28.
[14] D. Baciu, J. Simitzis, J. Optoelectron. Adv. Mater. 9 (2007) 3320–3324.
[15] P. Siriphannon, Y. Kameshima, A. Yasumori, K. Okada, S. Hayashi, J. Eur. Ceram. Soc. 22 (2002) 511–520.
[16] A.G. Kalampounias, N. Bouropoulos, K. Katerinopoulou, S.N. Yannopoulos, J. Non-Cryst. Solids 354 (2008) 749–754.
[17] A. Meiszterics, K. Sinkó, Colloids Surf., A 319 (2008) 143–148.
[18] K. Sinkó, A. Meiszterics, L. Rosta, Progr. Colloid. Polym. Sci. 135 (2008) 130–138.
[19] A. Meiszterics, L. Rosta, H. Peterlik, J. Rohonczy, S. Kubuki, P. Henits, K. Sinkó, J. Phys. Chem. A 114 (2010) 10403–10411.
[20] T. Kokubo, H. Kushitani, S. Sakka, T. Kitsugi, T. Yamamuro, J. Biomed. Mater. Res. 24 (1990) 721–734.
[21] M. Figueiredo, J. Henriques, G. Martins, F. Guerra, F. Judas, H. Figueiredo, J. Biomed. Mater. Res. B: Appl. Biomater. 92 (2010) 409–419.
[22] S.T. Li, H.C. Chen, D. Pierson, D. Yuen, P. Hansen, NuOss™, a Bone Grafting Material for Oral Surgery: A Comparative Study with BioOss. Available from URL: http://www.stomascience.com/uploads/documents/Research/Comparative%20Study%20with%20BioOss.pdf.
[23] E. Dahi, H. Bregnhøj, 1st International Workshop on Fluorosis Prevention and Defluoridation of Water; 1st Proceedings (2010) 96–103.
[24] H.B. Breitz, R.E. Wendt, M.S. Stabin, S. Shen, W.D. Erwin, J.G. Rajendran, J.F. Eary, L. Durack, E. Delpassand, W. Martin, R.F. Meredith, J. Nucl. Med. 47 (2006) 534–542.
[25] S. Hall, Basic Biomechanics, Fifth edition McGraw-Hill Humanities/Social Sciences/Languages, 2007.
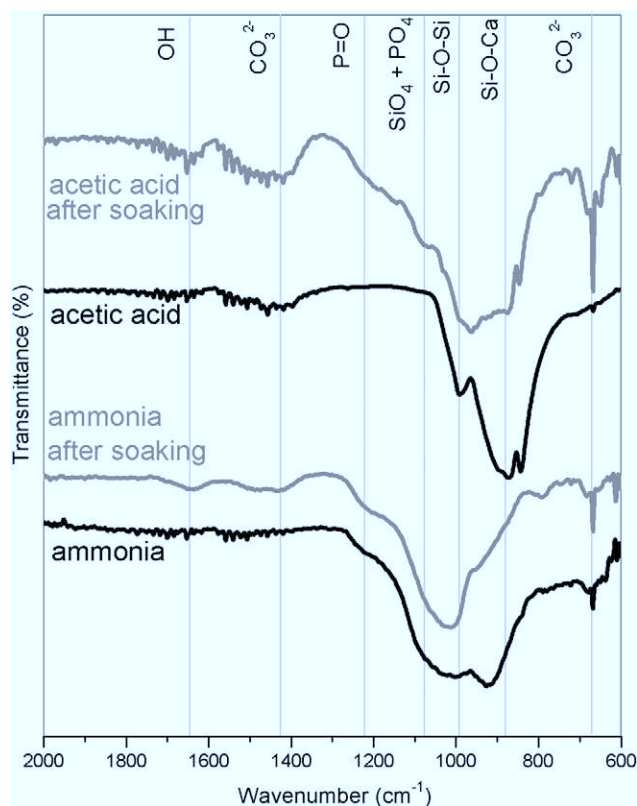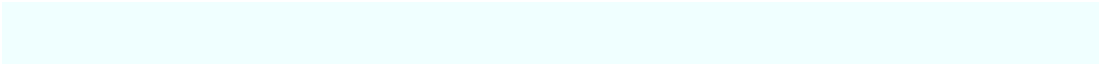[26] Z.B. Friedenberg, W.H. Simon, Surg. Gynecol. Obstet. 116 (1963) 588–592.

Fig. 9. FTIR spectra of bulk ceramics sintered and soaked in SBF.

[27] S. Hulbert, in: A.L. Bement Jr. (Ed.), Biomaterials, University of Washington Press, Seattle, 1971, pp. 3–77.

[28] I. Izquierdo-Barba, M. Colilla, M. Vallet-Regí, J. Nanomater. 2008 (2008) 1–14.

[29] S.V. Dorozhkin, Materials 2 (2009) 399–498.

[30] D.M. Liu, Mater. Chem. Phys. 36 (1994) 294–303.

[31] P.N. De Aza, F. Guitian, S. De Aza, Scr. Metall. Mater. 31 (1994) 1001–1005.

[32] I. Izquierdo-Barba, M. Vallet-Regi, J. Biomed. Mater. Res. 47 (1999) 243–250.

[33] P.N. De Aza, Z.B. Luklinska, M. Anseau, F. Guitian, S. De Aza, J. Dent. 27 (1999) 107–113.

[34] M.M. Pereira, L.L. Hench, J. Sol-Gel Sci. Technol. 7 (1996) 59–68.